Investigation of NanoSQUIDs Fabricated with a Range of Focused Ion Beam Sources

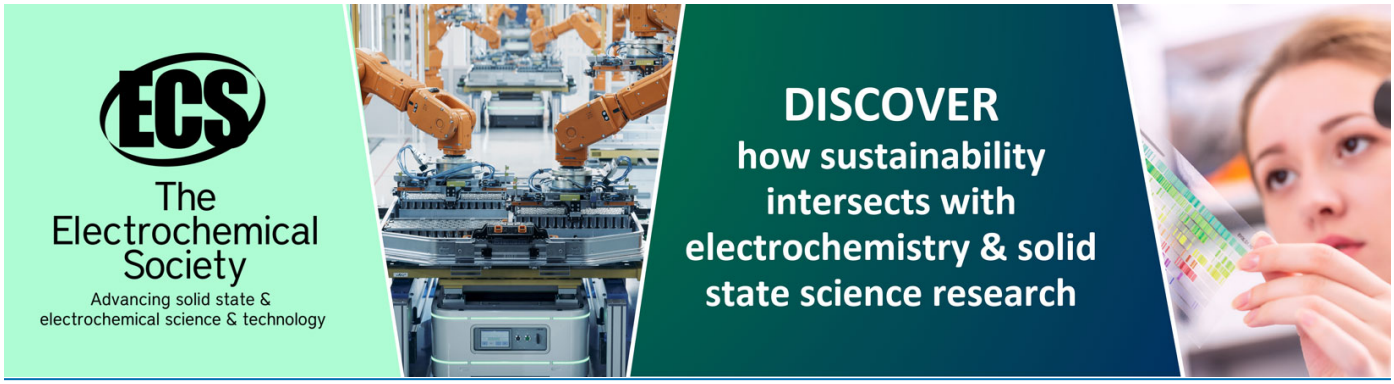

Investigation of NanoSQUIDs Fabricated with a Range of Focused Ion Beam Sources

E Polychroniou[1,2], J Gallop[1], T Godfrey[1,3], D Cox[1], G Long[1], J Chen[4], E Romans[3] and L Hao[1,2]

[1]National Physical Laboratory, Teddington, TW11 0LW, UK

[2]Materials Department, Imperial College London, London SW7 2AZ, UK

[3]London Centre for Nanotechnology, University College London, London WC1H 0AH, UK

[4]Department of Mechanical and Aerospace Engineering, Brunel University, Uxbridge UB8 3PH, UK

e-mail: ling.hao@npl.co.uk

Abstract. SQUIDs (Superconducting Quantum Interference Devices) are macroscopic quantum devices capable of detecting and measuring a wide variety of physical parameters with unprecedented sensitivity. SQUIDs based on nanobridge weak links have shown increasing promise for quantum information and quantum sensing applications such as single spin detection. Focussed ion beam etched nanobridges have properties which can enhance nanoSQUID device performance but are often limited in terms of their non-hysteretic operating temperature range. Here we describe measurements of FIB-milled nanobridges, as single weak links or in nanoSQUIDs, made using either Ga, Xe or Ne ion beam sources. Their properties as a function of temperature, bias current, magnetic field and microwave power are measured and modelled according to a range of superconductivity models, as a means for improved understanding of the associated nanobridge parameters. We further propose techniques to extend the non-hysteretic operating temperature range of the devices.

1. Introduction

As superconducting devices extend their regimes of application to lower temperatures, as demanded by quantum technologies, and to smaller length scales, as demanded by nanoscience, the workhorse trilayer Josephson junctions [1-3] are increasingly challenged. Other superconducting electronic technologies for fabricating Josephson junctions may have advantages in these areas but may also suffer from different limitations. In this paper we present results for nanobridge junctions fabricated in single layer Nb films using a focused ion beam (FIB) to etch the film down to the nanoscale. We present results on junctions and SQUID devices fabricated with three different ion beam sources (Ga, Xe and Ne), demonstrating their resistance as a function of temperature (R-T), current-voltage characteristics (I-V) and the observation of microwave induced Shapiro step characteristics. We aim to extract underlying processes to explain the differences and similarities in the properties of these differently fabricated nanobridge junctions.

The devices are being developed for a range of quantum mechanical applications [4-6], including attempts at single spin detection [7-11], number resolved single photon detection [12] and integration with nanoelectromechanical systems (NEMS) resonators [13-15]. The SEM images shown in Fig. 1 serve to illustrate the wide variation of single layer structures which we are fabricating. Any one of the three ion beam sources can be used to fabricate any one of the generic designs but here we have selected one of each of the three ion beam examples.

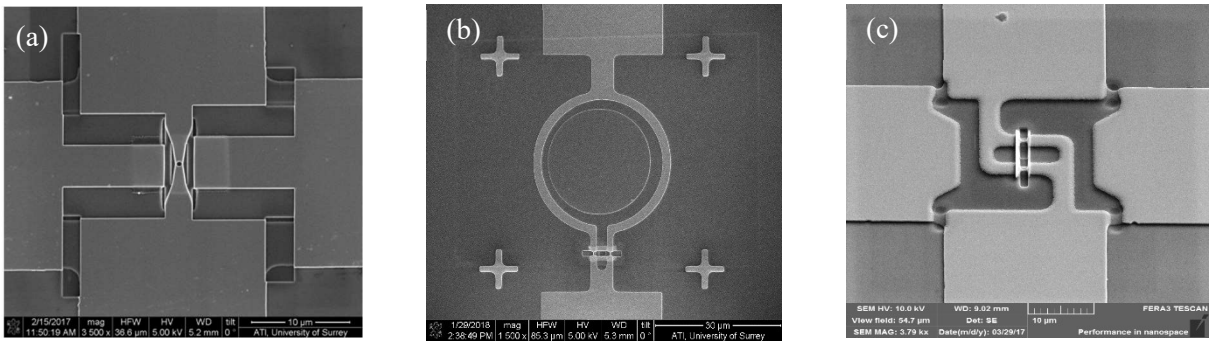

Figure 1. SEM images of three SQUID-based devices fabricated from single layer Nb films (200 nm thick): (a) nanoSQUID for single spin detection fabricated with Ga FIB, (b) ISTED SQUID based single photon based detector fabricated using Ne FIB, and (c) slotted nanoSQUID design for NEMS detection fabricated with Xe FIB.

2. Fabrication and Measurement Methods

The Nb films (~200 nm thick) are sputter deposited on a Si substrate with 200 nm of SiO_2. Coarse patterns of tracks and contact pads and larger SQUID loops are made using conventional photolithography. Up to eight SQUID devices are patterned on each chip, depending on the layout required. For Inductive Superconducting Transition Edge Detectors (ISTED) there are 12 devices patterned in a 5 mm x 5 mm chip. The nanoscale patterning is carried out by the selected FIB system. The ion beams used are either Ga (Ga sputter yield is 3.89, average range is 11.5 nm and onset dose is 2.56×10^{14} ions/cm^2), Xe (Xe sputter yield is 5.68, average range is 8.6 nm and onset dose is 1.76×10^{14} ions/cm^2), or Ne (Ne sputter yield is 0.99, average range is 28 nm and onset dose is 1.01×10^{15} ions/cm^2). Three beams are at 30 kV into Nb at normal incidence. Constrictions down to a width and length of ~50 nm were fabricated with each system.

Following FIB etching the chips are mounted on a chip holder and wire bonded before mounting on the cold plate of a low noise pulse tube cooler. The cooler has a base temperature of 2.7 K and is provided with microwave cabling and a 5 T superconducting magnet. The copper cold plate on which the chip holder is mounted can be temperature controlled from 3 K to ~ 20 K using a calibrated Cernox temperature sensor and precision temperature controller providing sub-mK temperature stability.

Measurements are carried out using conventional dc biasing techniques with low noise room temperature amplifiers. Flux modulation is provided by the 5 T superconducting magnet, the chip is placed in the centre of the solenoid perpendicular to the magnetic field. The chip can be irradiated with microwave power at a frequency provided by a synthesized microwave source which is tunable from 10 MHz to 6 GHz transmitted by a semi-rigid cryogenic cable terminated in an antenna located close to the chip surface.

3. Results and Analysis

3.1. Resistance versus Temperature (R-T) Plots

To test the devices on each chip the first measurement is a 4-terminal determination of the SQUID resistance *R* as a function of temperature *T*. Fig. 2 shows typical *R-T* curves for each of the three different types of nanobridge junction, according to the ion type used for milling.

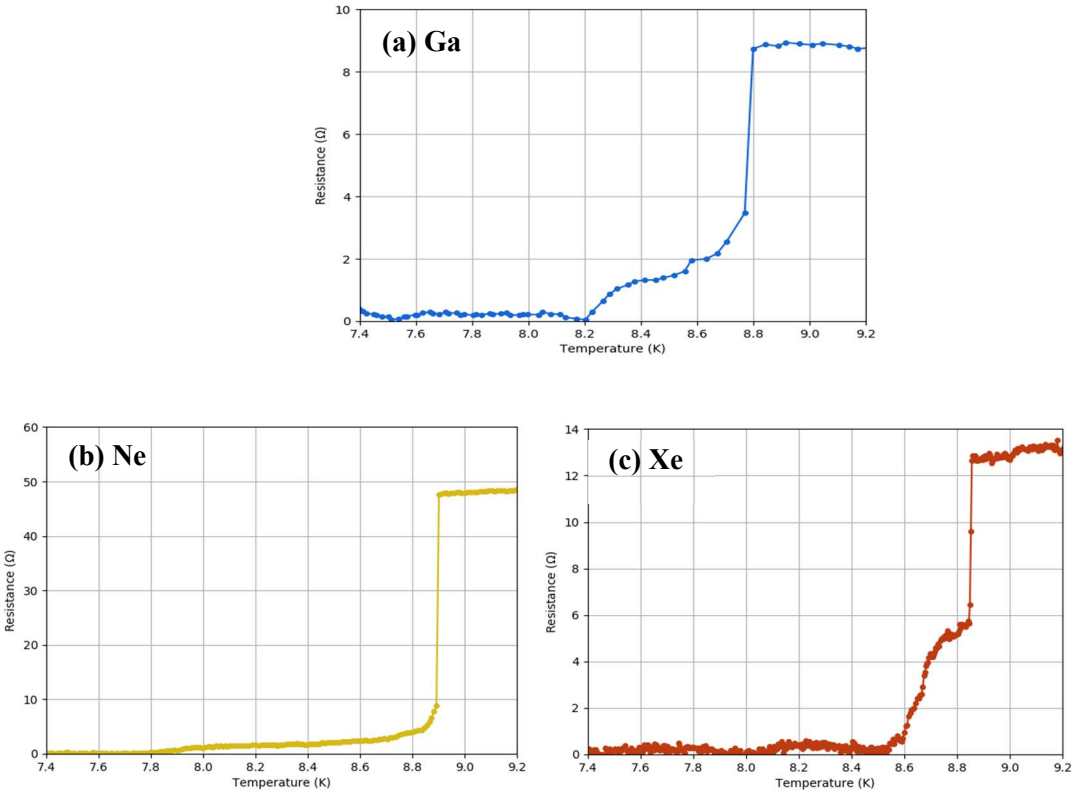

Figure 2. *R-T* characteristics of three SQUIDs: (a) Ga FIB fabricated SQUID with 300 nm loop diameter, (b) Ne FIB fabricated ISTED device with 25 μm diameter SQUID loop, (c) Xe FIB fabricated slotted nanoSQUID device with a 10 x 3 μm slot.

All three SQUID types show some similarities, for example the onset of superconductivity in the strongly superconducting thin film tracks begins at around 8.8 K, with a sharp drop in resistance to a small value over a transition width of ~10 mK. Below this region each SQUID type shows a slow decline to zero resistance over a range of 0.25 K to 1.5 K, the smallest range being for the Xe SQUID and the largest being for the Ne SQUID. The total resistance change over this slow decline is between 2 Ω and 5 Ω for the three different types. We interpret the zero resistance state as the onset of superconductivity in the nanobridges of the SQUIDs.

3.2. Current-voltage characteristics (IVC) of the SQUIDs

Our Nb nanobridge SQUIDs show dc current voltage characteristics which are very close to that of overdamped resistively shunted junctions (RSJ) when measured within around 0.5 K of the initial zero resistance temperature as shown in Fig. 3. The agreement with this model is consistent with the nanobridge junction shunt capacitance being negligible for coplanar superconducting electrodes. At lower temperatures the transition from zero to finite voltage at the critical current takes on a sharp jump

and the IVC becomes hysteretic, as shown by the IVC for increasing current being different from the current decreasing IVC. This behaviour is well understood for nanobridge junctions due to the formation of hot spots in the normal state where the phase difference across the junctions becomes indeterminate. At low enough temperatures these can be sustained by a current below the critical current leading to hysteresis. One aspect of optimising the performance of these SQUIDs involves trying to design the nanobridges (for instance with a normal metal overlayer) to extend the non-hysteretic region as much as possible to lower temperatures in order to extend the SQUID operating temperature range using conventional readout.

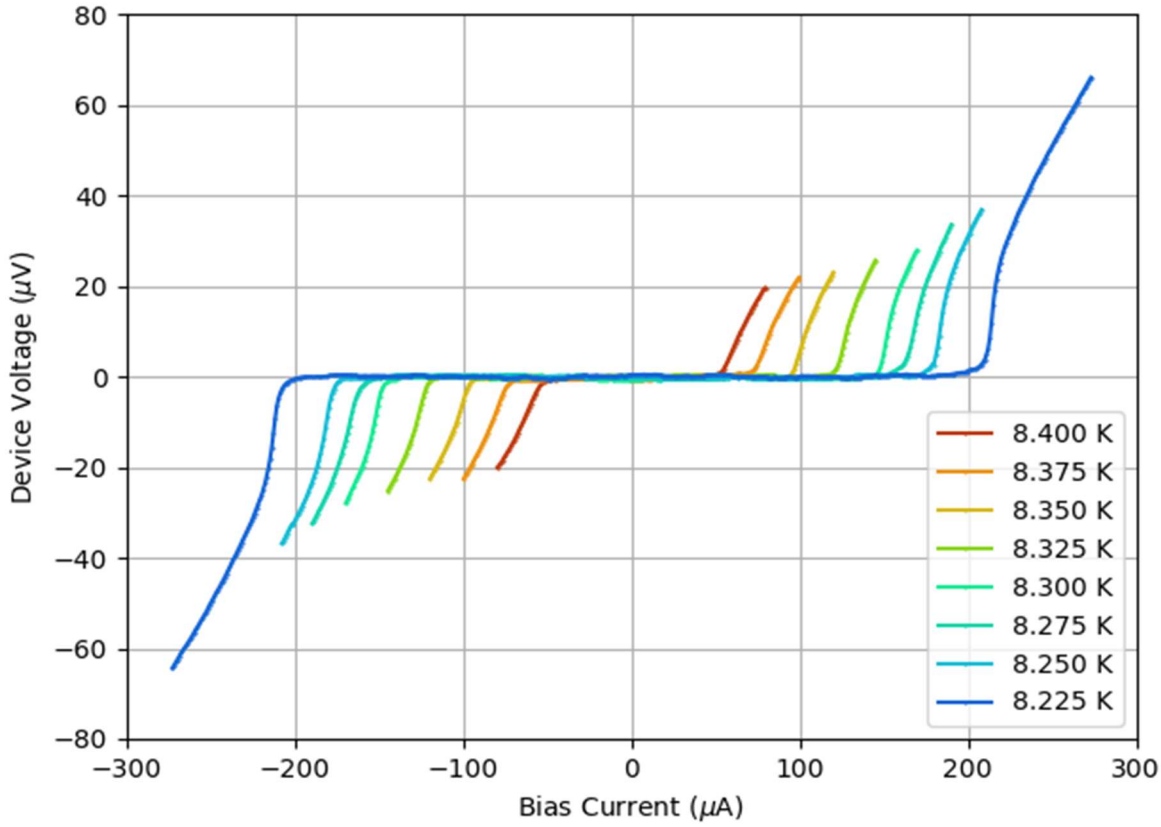

Figure 3. *I-V* curves as function of the temperature for a Ga FIB device (Ga-S5-D30-2).

Measurements of the critical current as a function of temperature for a selection of SQUID devices fabricated using the different ion beam sources are shown in Fig. 4. While this represents a relatively small sample of devices it is interesting that the Xe SQUIDs show, on average, the most rapid increase in critical current with falling temperature, the Ne SQUID shows the slowest rise with the Ga device average being intermediate. In addition, the extrapolated T_c for zero critical current shows a similar trend, being highest for Xe and lowest for Ne. We speculate that the observed behaviour correlates with the relative atomic mass units of the ions used for milling. Thus neon has an ionic mass of 20, gallium 70 and xenon 131. Intuitively one might expect that the heavier an ion the more damage it would do to the Nb crystal lattice and that lattice disruption would tend to suppress superconductivity. Our results suggest that the opposite is the case, but it is necessary to consider not only the damage caused by a single ion but the total amount of ion dose required to remove the same amount of material. Thus since the sputter yield for Ne is as much as four times less than for Ga or Xe and its range is longer, it will remove much less material per collision so that the total dose required will be much greater and more penetrating, resulting in an effectively smaller junction with lower T_c.

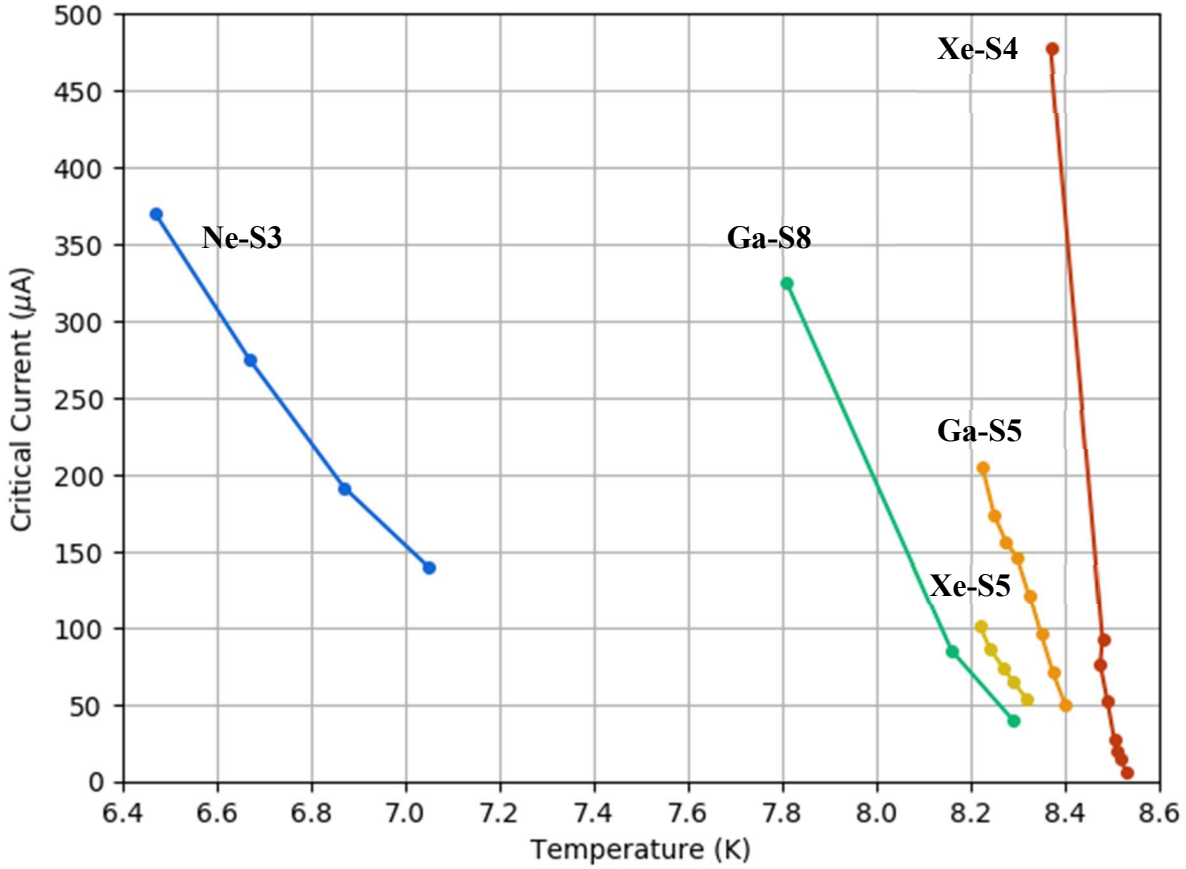

Figure 4. Critical Current I_c versus temperature T for five FIB devices fabricated by different ions as indicated in the figure.

4. Microwave Response and Shapiro Steps

We have recently begun to develop microwave readout methods to interrogate these nanobridge nanoSQUIDs. It is well known that for SIS tri-layer Josephson junctions when dc biased beyond the critical current with mean dc voltage of V across the junction there will be an ac supercurrent flowing through the junction with frequency $f = 2eV/h$ where $2e$ is the pair charge and h is Planck's constant. It was shown very early after Josephson's original paper that when a junction is current-biased in the finite voltage regime is irradiated with microwaves at frequency f a series of equally spaced constant-voltage Shapiro steps are induced in the IVC, each one occurring at a voltage $V_n = nhf/2e$, n being integer [16-17]. The steps V_n occur whenever the internal ac Josephson frequency is harmonically related to nf. The observation and measurement of Shapiro steps provides a useful means to characterise the high frequency properties of Josephson junctions. Shapiro steps are equally observed in dc SQUIDs as well as in single junctions, so we have made measurements on the step profiles in the IVCs of each of our SQUID types when irradiated with microwaves at around 5 GHz. The amplitudes of the induced steps increase as the microwave power is increased until a maximum for each is reached, beyond which the amplitudes oscillate. The maximum step number n_{max}, which is detectable, gives an indication of the maximum frequency at which a supercurrent can flow in our SQUIDs.

The RSJ model may be readily solved analytically for dc bias situations. But when a microwave external current is included in addition to the conventional dc bias current, a numerical model must be used, which now incorporates two junctions (which could have identical or different critical currents and shunt resistances as necessary) as well as a normal distribution of noise voltages across the junctions.

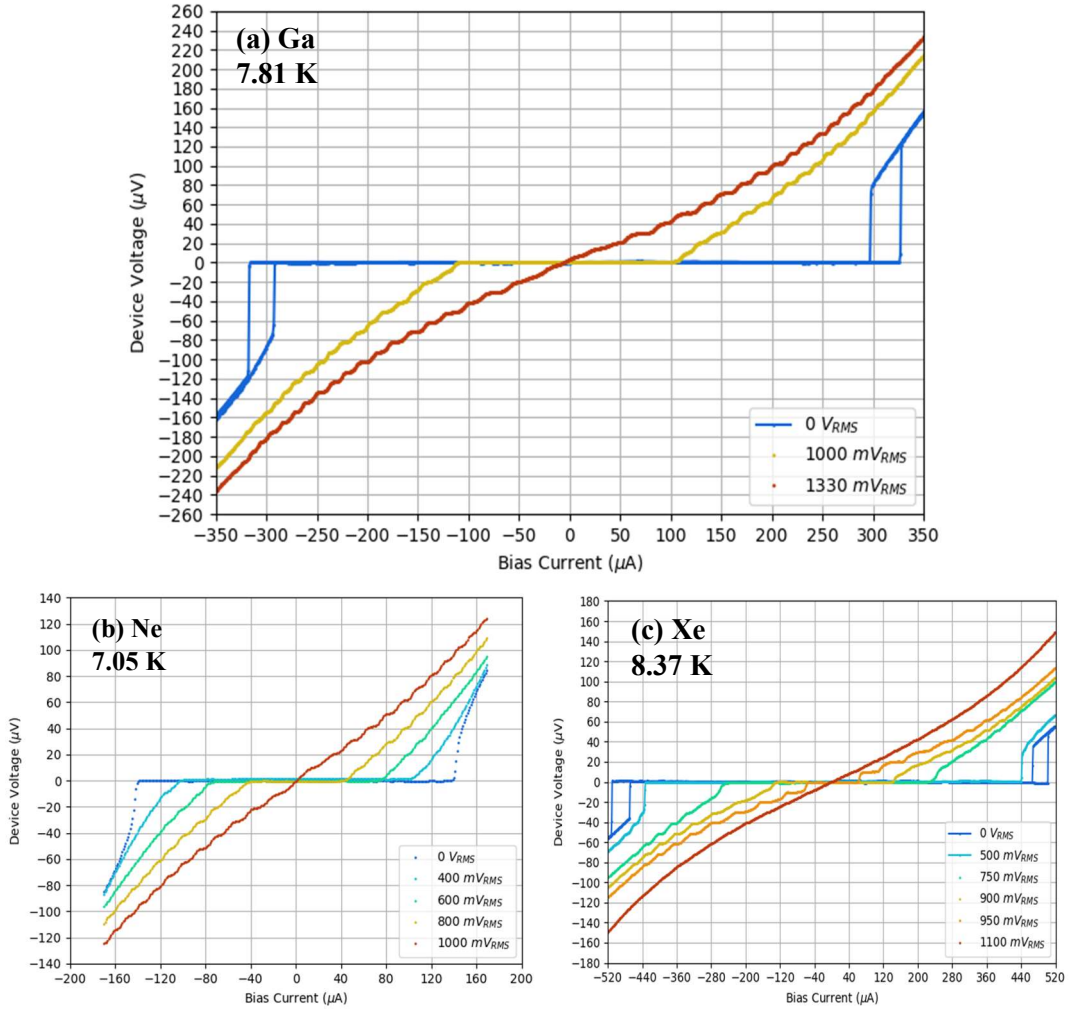

Figure 5. Experimental IVC plots for each of the three SQUID types showing the effect of increasing amplitudes of microwave current applied to the SQUIDs: (a) Ga FIB device, (b) Ne FIB device, (c) Xe FIB device. The temperatures were selected to give a wide range of Shapiro steps.

We model the d.c. SQUID directly with two identical Josephson junctions having equal critical currents and shunt resistances. Then the coupled second order differential equations for the time dependent phases of the two are solved over a time interval corresponding to many cycles of the Josephson oscillation. A sine wave current is added to the d.c. bias current to represent the applied microwave signal. Carrying out a time average of the phase difference versus time for these solutions provides a d.c. voltage across the SQUID. Then by running the model repeatedly with different d.c. bais currents the entire IVC may be calculated for a range of bias currents and rf current amplitudes. Noise rounding was also added to the model by introducing random noise voltages with a Gaussian distribution.

The IVCs fit very closely to such a model with identical junction parameters, particularly in the temperature region just below the nanobridge transition temperature. The behaviour of the induced Shapiro steps with increasing microwave power is well modelled. Fig. 6 shows an example of the close agreement between experiment and theory for a Ga FIB fabricated SQUID for zero rf current and two

higher amplitude values. At voltages above around 60 μV at this temperature the upward curvature of the IVC departs from the RSJ model and this is shown for all three SQUID types. This probably indicates the increased effective temperature of the junctions at higher bias currents, with a corresponding reduction of the Josephson supercurrent.

5. Conclusion

This paper presents results on three different methods for processing single layer nanoSQUIDs based on three different focused ion beams. The overall conclusion answers a long-standing question regarding the influence of implanted ions on the junction. The low mass Ne ions must provide much higher dose than the more massive ions, leading to deeper damage within the film. The resulting junction region will be smaller on account of this, leading to lower T_c and a flatter change in I_c with temperature. Ga, unlike the noble gases involved in the other two ion sources, is expected to implant and form chemical bonds which might be expected to alter the superconductivity properties of the junctions. But our results suggest this is not a significant effect.

Our modelled results are in good agreement with what is observed for real junctions, except that at high frequencies the observed step width begins to fall below the values predicted by the RSJ model, indicating that there is an upper limit to the oscillating frequency. For a tunnel junction this is of order $2\Delta(T)/e$ where $\Delta(T)$ is the temperature dependent junction gap parameter. For our nanobridges there is no such simple expression and we treat the upper frequency as a parameter to be deduced from comparing experiment with theory. The microwave induced Shapiro results indicate that the upper frequency response of the nanobridge junctions extend to a temperature dependent upper limit, of order the critical frequency $f_{crit} = RI_c/\Phi_0$. As the temperature is reduced we observe departures from the RSJ model at high bias currents. The upward curvature of the IVC probably indicates extra heating, leading to a reduction in the Josephson supercurrent amplitude. Reassuringly for the future application of these junctions for microwave SQUID operation, the upper frequency limit at all operating temperatures for all three different SQUID types appears to be above 50 GHz.

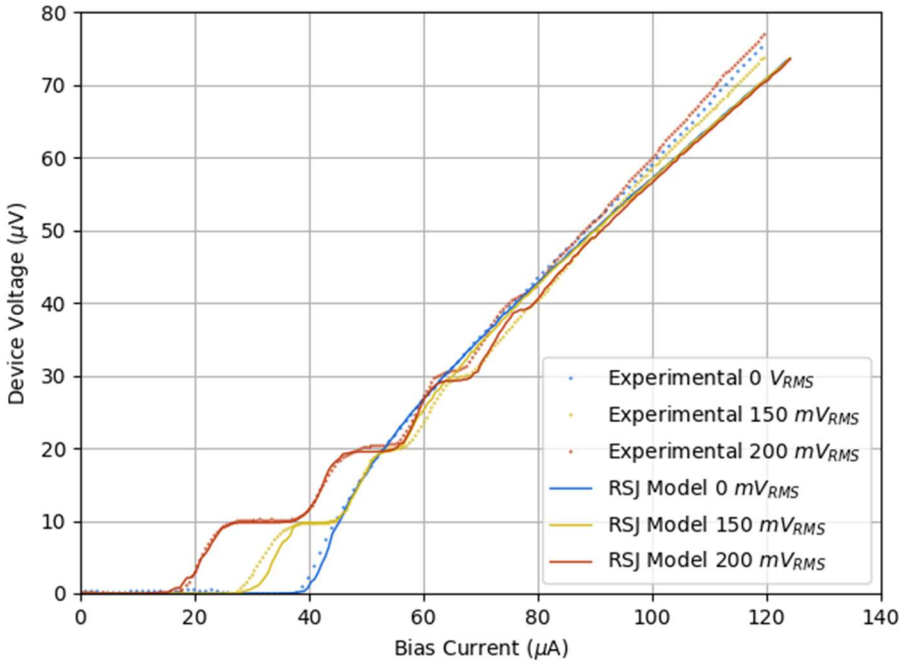

Figure 6. IVCs at temperature of 8.29 K for three different microwave power levels, including both experiment and RSJ model fits amplitude for Ga FIB S8-Device 20.1.

Acknowledgements
This work was supported in part by the UK National Measurement System, the EU project EMPIR 17FUN06 SIQUST (the EMPIR programme is co-financed by the Participating States and from the European Union's Horizon 2020 research and innovation programme); and by the UK Engineering and Physical Sciences Research Council (EPSRC), and UCL Impact Studentship. We thank NIM (China) for help with Nb thin film growth and photolithographic patterning.

References
[1] Clarke J and Braginski A I 2004 The SQUID Handbook: Fundamentals and Technology of SQUIDs and SQUID Systems, (Weinheim, Germany:Wiley) vol.1
[2] Niemeyer J, Grimm L, Meier W, Hinken J H and Vollmer E 1985, Appl. Phys. Lett. **47** 1222-1223
[3] Granata C, Vettoliere A, Russo R, Fretto M, De Leo N and Lacquaniti V 2013 *Appl. Phys. Lett.* **103** 102602
[4] Hao L and Granata C 2017 *Supercon. Sci. Technol.* **30** 050301
[5] Foley C P and Hilgenkamp H 2009 *Supercond. Sci. Technol.* **22** 064001
[6] Granata C and Vettoliere A 2016 *Phys. Rep.* **614** 1– 69
[7] Wernsdorfer W 2009 *Supercond. Sci. Technol.* **22** 064013
[8] Lam S K H and Tilbrook D L 2003 *Appl. Phys. Lett.* **82** 1078-80
[9] Hao L, Aßmann C, Gallop J C, Cox D, Ruede F, Kazakova O, Josephs-Franks P, Drung D and Schurig Th. 2011 *Appl. Phys. Lett.* **98** 092504
[10] Vasyukov D, Anahory Y, Embon L, Halbertal D, Cuppens J, Neeman L, Finkler A, Segev Y, Myasoedov Y, Rappaport M L, Huber M E & Zeldov E 2013 *Nat. Nanotechnol.* **8** 639-644
[11] Martínez-Pérez M J, Gella D, Müller B, Morosh V, Wölbing R, Sesé J, Kieler O, Kleine R and Koelle D 2016 *Jnl. Chem. Phy.s* **10** 8308–8315
[12] Gallop J, Cox D and Hao L 2015 *Supercond. Sci. Technol* **28** 084002
[13] Hao L, Cox D C, Gallop J C, Chen J, Rozhko S, Blois A and Romans E J, 2013 *IEEE Trans. Appl. Supercond.* **23** 1800304
[14] Bechstein S, Ruede F, Drung D, Storm J-H, Kohn C, Kieler O F, Kohlmann J, Weimann T, Patel T, Li B, Cox D, Gallop J C, Hao L and Schurig T 2015 *IEEE Trans. Appl. Supercond.* **25** 1602604
[15] Patel T, Li B, Li T, Wang R, Gallop J, Cox D, Romans E J, Chen J and Hao L 2017 *IEEE Trans. Appl. Supercond.* **27** 1602005
[16] Vanneste C, Chi C C, Gallagher W J, Kleinsasser A W, Raider S I, and Sandstrom R L 1988 *Jnl. Appl. Phys.* **64** 242-45
[17] Shelly C D, See P, Ireland J, Romans E J and Williams J M 2017 *Supercond. Sci. Technol* **30** 095013